Received 29 May 2022; accepted 16 June 2022. Date of publication 5 July 2022; date of current version 12 August 2022.

Digital Object Identifier 10.1109/OJAP.2022.3188693

Forward and Inverse Scattering of Metallic Objects Through Focused Bessel-Shaped Fields

SANTI C. PAVONE (Senior Member, IEEE), GINO SORBELLO (Member, IEEE), AND LORETO DI DONATO (Member, IEEE)

(Invited Paper)

Department of Electrical, Electronics and Computer Engineering, University of Catania, 95125 Catania, Italy

CORRESPONDING AUTHOR: L. DI DONATO (e-mail: loreto.didonato@unict.it)

ABSTRACT This paper deals with both forward and inverse electromagnetic scattering of metallic objects by focused Bessel-shaped incident field. After discussing the main features of this kind of field, it is shown that its focusing capabilities may offer new effective possibilities for the detection of metallic targets which are not so far extended with respect to the probing wavelength, i.e., not satisfying the hypotheses of physical optics approximation. Numerical examples are performed by means of full-wave simulations, and then inversion algorithms based on back-propagation and physical optics are exploited to show that more accurate reconstructions can be pursued using Bessel-shaped fields.

INDEX TERMS Inverse scattering, forward scattering, Bessel-shaped fields, focusing, microwave imaging, physical optics, singular value decomposition.

I. INTRODUCTION

SOME electromagnetic (EM) problems in engineering and physics require the mitigation of unavoidable beam diffraction, such as imaging applications [1]–[5], near-field focusing, ground penetrating radars (GPR) [6]–[8], near-field high-data rate transfer [9], small particle manipulation [10], [11], just to mention a few. Hence, focused and collimated beams have gained increasing interest, especially in the last decades. Under this perspective, so-called non-diffractive waves have been studied both theoretically and experimentally [12]–[14], namely a family of exact solutions of Helmholtz equation characterized by high field collimation and spatial confinement. Moreover, in 1987 Durnin and his research group introduced a subclass of nondiffractive waves, namely Bessel beams [8], [15], [16], i.e., ideal nondiffractive solutions of Helmholtz equation in cylindrical coordinates, characterized by field focusing and concentration in its main lobe, in which the wavefront is locally planar.

Shape reconstruction of strongly scattering objects, such as metallic ones, or high-contrast dielectric targets, is one of the most important challenges in microwave and remote sensing applications, such as GPR, nondestructive testing, underground mapping utilities, demining of unexploded ordnances, imaging of metallic rods in concrete pillars and subsurface voids. Unfortunately, such a goal entails to solve a non-linear problem, which can be tackled as an iterative optimization task and requires also some regularization strategies to counteract ill-posedness of the problem [17]. One possible way to escape from this drawback is to consider linearized approaches based on physical optics (PO), or high-frequency Kirchhoff approximation, to reconstruct shape of unknown metallic objects starting from the knowledge of the measured scattered field. However, it should be mentioned that generally PO provides accurate results only when the scatterer's radius of curvature is sufficiently larger than the probing wavelength and when mutual scattering effects between different parts of the same target, or among multiple targets, are negligible [18]. As a result, PO approximation can be used only for imaging large convex targets. In the light of the above, a Bessel-shaped field (BF) seems to be attractive because it may improve, under certain hypotheses, the PO approximation when target extents are comparable with the probing wavelength (only few wavelengths), or when they exhibit concavity or multiple scattering phenomena.

According to the above assumptions, in [19] we have analytically derived the scattering of a perfect electric conducting (PEC) cylinder by a Bessel beam through plane-wave field expansion. Moreover, it has been also proven that the

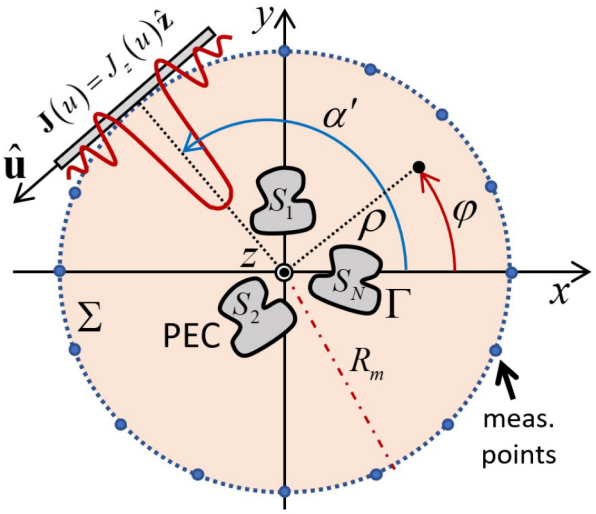

FIGURE 1. Reference geometry for both direct and inverse scattering problems. A system of unknown PEC scatterers is illuminated by a focused Bessel-shaped field. The scattered field by obstacles is collected by point-like receivers, placed on a measurement circle of radius R_m.

validity of standard PO approximation can be extended to PEC cylindrical scatterers whose dimension is comparable with probing wavelength.

In this work, we investigate the capability of a BF in imaging the support of metallic targets, which does not belong to the range of PO approximation. In this respect, we consider two well-known imaging approaches, i.e., the back-propagation reconstruction scheme and a PO inversion strategies based on singular value decomposition (SVD) of the relevant operator mapping data-to-unknown relationship. In particular, in the case of PO-based shape reconstruction, the use of focused beams allows catching some features of the scattering system that are completely blurred when the classical plane-wave assumption is used as illuminating field in the region of interest. Such an advantage can be profitably used to improve results in some specific applications such as non destructive testing of materials (NDT), GPR and near field radar application in the millimeter and sub-millimeter wave spectrum.

The paper is divided as follows; in Section II, the formulation of the forward scattering problem is discussed and the main features of BFs are discussed. In Section III, the formulation of the inverse scattering problem is introduced and the adopted inversion strategies are briefly illustrated. In Section IV imaging results for different metallic targets are shown and compared versus standard plane-wave (PW) illumination. Finally, conclusions are drawn.

II. DIRECT PROBLEM FORMULATION

The geometry of the 2D problem is depicted in Fig. 1, in which a system of unknown PEC scatterers in a background medium is illuminated by a BF. The primary source of length L is characterized by a rotating auxiliary uv reference system, in which $\hat{\mathbf{u}}' = -\sin\alpha'\hat{\mathbf{x}} + \cos\alpha'\hat{\mathbf{y}}$ denotes the unit vector describing the source orientation, while the measurement points are placed on a circle of radius R_m. In the following, both incident BF and scattered fields are described in detail.

A. INCIDENT BESSEL-SHAPED FIELD

By assuming a transverse-magnetic illumination with respect to the z-direction (TM^z) [20] and the time-harmonic convention $\exp(j\omega_0 t)$, being ω_0 the operating angular frequency, a z-polarized electric current density described by

$$\mathbf{J}^{BF}(u) = J_z^{BF}(u)\hat{\mathbf{z}} = H_0^{(1)}\left(k_{\rho a}u\right)\Pi\left(\frac{u}{L}\right)\hat{\mathbf{z}}, \tag{1}$$

is imposed on the primary source distribution, i.e., shaped as a truncated zeroth order first kind Hankel function $H_0^{(1)}(\cdot)$. In (1), $k_{ua} = k\sin\theta_a$ is the imposed wavenumber on the primary current distribution, $k = \omega_0/c$ the free-space wavenumber, and θ_a the axicon angle describing the BF [15], [21], while $\Pi(\frac{u}{L})$ denotes the rectangular function of width L centered at $u = 0$. Such an inward cylindrical traveling wave distribution is able to radiate a focused BF in the xy plane. Indeed, the radiated field can be asymptotically expanded in terms of geometrical optics contributions (rays), by resorting to the EM field high-frequency approximation. The inward and outward ray-optical contributions interfere each other in the xy plane and synthesize a BF, by exploiting the same physics phenomenon behind so-called *axicon lenses* (with the exception of the azimuth symmetry in the 2D problem at hand), widely used in optics [22], [23]. It is worth noting that an inward cylindrical current distribution $H_0^{(1)}(k_{ua}u)\Pi(u/L)$ has been preferred with respect to more standard truncated zeroth order Bessel function, namely $J_0(k_{ua}u)\Pi(u/L)$. This latter because in [24] it has been proven that such an aperture distribution theoretically allows wider operating ranges in terms of beam purity and bandwidth (i.e., no bandwidth lower-bound exists in principle), hence it can be profitably exploited also for further improvements of the proposed method.

The truncation due to primary source finite extent, taken into account by the rectangular function in (1), bounds the maximum achievable distance by the BF beyond which it starts spreading out and lose their collimation. Such a distance is normally referred in literature as *nondiffractive range* (NDR), and depends on the density distribution current length L and on the axicon angle θ_a. The exact closed-form expression of the NDR can be analytically derived in the 3D radiation problem ($L/2\cot\theta_a$), but in the 2D case it is only approximated. However, to describe the main feature of BFs, we refer to the half-power beamwidth normalized to the wavelength (HPBW$_\lambda$), i.e.,

$$\mathrm{HPBW}_\lambda = \frac{\mathrm{HPBW}}{\lambda} = \frac{0.48}{\sin\alpha_a},$$

in which $\lambda = 2\pi/k$ is the operating wavelength. It is worth noting that HPBW$_\lambda$ plays a crucial role in designing the scattering measurement setup as it gives a metric to ensures that the scattering system is properly illuminated by the incident BF. In this respect, since the scattering system is unknown, some prior information about the nature of the

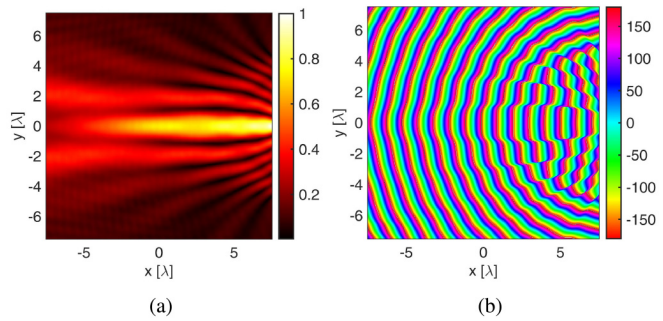

FIGURE 2. (a) Normalized amplitude and (b) phase of an incident BF characterized by an axicon angle $\theta_a = 15°$ and radiated by a $\hat{y}$-directed linear source of length $L = 10\lambda$, placed at $x_a = 7.5\lambda$ with respect to the global Cartesian reference system.

inspected scenario is useful to set up the BF with adequate HPBW_λ. Moreover, the possibility to exploit radiating structures able to synthesize more than one BF at different axicon angles, may represent an interesting chance which can be exploited in further works, but it is out of the scope of the present paper.

Due to TM^z field expansion, the electric BF can be fully characterized only by its z-component, namely $\mathbf{E}_i^{BF}(\boldsymbol{\rho}) = E_i^{BF}(\boldsymbol{\rho})\hat{\boldsymbol{z}}$, so that

$$E_i^{BF}(\boldsymbol{\rho}) = \int_{-\infty}^{+\infty} J_z^{BF}(\boldsymbol{u}') H_0^{(2)}\big(k|\boldsymbol{u}' - \boldsymbol{\rho}|\big) d\boldsymbol{u}', \tag{2}$$

in which $H_0^{(2)}(\cdot)$ denotes the zero-th order second kind Hankel function and $u' = \sqrt{(x')^2 + (y')^2}$ the generic source point. To provide a visual description of the proposed incident field, in Fig. 2 a numerical example is provided, in which a radiating linear current density distribution of $L = 10\lambda$, whose center is at $(x_a, y_a) = (7.5, 0)\lambda$, radiates a BF characterized by an axicon angle $\theta_a = 15°$. In Fig. 2(a) (resp. 2(b)), the radiated electric field magnitude (phase) is shown. As it can be inferred, the field is well-collimated inside the main lobe up to NDR $\approx 13\lambda$, beyond which it loses its focusing properties. As concerns the phase plot, it can be argued that the local wavefront inside the main lobe is planar. In the following, the scattered field by an incident BF is briefly described.

B. SCATTERED BESSEL-SHAPED FIELD

Under TM^z illumination, the scattered field by a system of PEC scatterers of the incident BF described by (1) is z-polarized, so that $\mathbf{E}_s^{BF} = E_s^{BF}\hat{\boldsymbol{z}}$. Moreover, by exploiting equivalence theorem [20], the scattered field, i.e., the field produced by re-irradiation of electric current densities induced on the scatterers, can be written as

$$E_s^{BF}(\boldsymbol{\rho}) = \int_\Gamma G\big(\boldsymbol{\rho}, \boldsymbol{\rho}''\big) J\big(\boldsymbol{\rho}''\big) d\boldsymbol{\rho}'', \tag{3}$$

in which $\Gamma = \Gamma_1 \cup \cdots \cup \Gamma_N$ is the union of N scatterer boundaries, $\boldsymbol{\rho}'' = \rho''(\cos\alpha''\hat{\mathbf{x}} + \sin\alpha''\hat{\mathbf{y}})$ the generic scattering point on Γ, $\mathbf{J}(\boldsymbol{\rho}'')$ the induced electric current density on Γ, and $G(\boldsymbol{\rho}, \boldsymbol{\rho}'')$ the 2D free-space scalar Green function, namely

$$G\big(\boldsymbol{\rho}, \boldsymbol{\rho}''\big) = \frac{1}{4j} H_0^{(2)}\big(k|\boldsymbol{\rho} - \boldsymbol{\rho}''|\big). \tag{4}$$

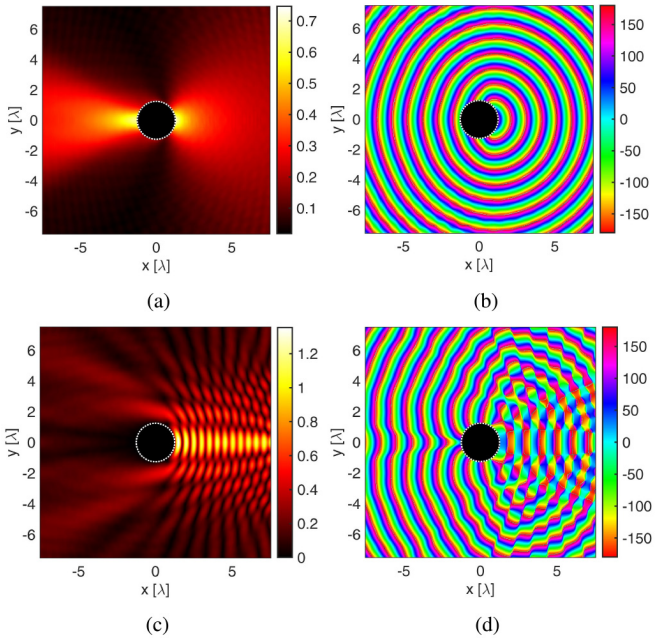

FIGURE 3. Scattering of a BF by a PEC cylinder of radius $R_c = 1.25\lambda$: (a) normalized amplitude (to the incident electric field maximum) and (b) phase of the scattered field; (c) normalized amplitude (to the incident electric field maximum) and (d) phase of the total field.

In Fig. 3(a) (resp. 3(b)), an example of scattered field magnitude (phase) of a focused incident BF by a PEC cylinder of radius $R_c = 1.25\lambda$ is shown. The scattered field magnitude is normalized to incident electric field maximum. From the magnitude plot, it can be inferred that the scattered field by a BF is localized in the neighborhood of the point in which it impinges, and also a forward scattering contribution can be noticed. Moreover, the phase plot allows understanding the physical mechanism of the scattering phenomenon; indeed, since the BF impinges in a localized portion of the scatterer, a localized electrical current density is in turn induced, so that the scattered phase resembles that of a cylindrical wave radiated by point like source in free space. For the sake of completeness, in Fig. 3(c) (resp. 3(d)) also the magnitude (phase) of the total electric field $\mathbf{E}_t^{BF}(\boldsymbol{\rho})$ is provided, in which the localized stationary pattern created by backward interference of incident and scattered fields is highlighted.

III. INVERSE PROBLEM FORMULATION

Inverse scattering of metallic targets aims at solving a coupled set of integral equations, composed by *i)* the scattered field (3) evaluated on a measurement line Σ parametrized by the vector $\boldsymbol{R}_m$, namely

$$E_s(\boldsymbol{R}_m) = \int_\Gamma G\big(\boldsymbol{R}_m, \boldsymbol{\rho}''\big) J\big(\boldsymbol{\rho}''\big) d\boldsymbol{\rho}'', \tag{5}$$

and *ii)* the magnetic field integral equation (MFIE) on (unknown) scatterer boundaries Γ,

$$J(\boldsymbol{\rho}) = J_i(\boldsymbol{\rho}) + \int_\Gamma \frac{\partial}{\partial \hat{\mathbf{n}}} G\big(\boldsymbol{\rho}, \boldsymbol{\rho}''\big) J\big(\boldsymbol{\rho}''\big) d\boldsymbol{\rho}'', \tag{6}$$

being $\hat{\mathbf{n}}$ the outwardly-oriented local normal to the scatterer boundaries, and $J_i(\boldsymbol{\rho})$ the electric current density. In (5)

and (6) the integrals denote the so-called "external" (or data) and "internal" (or object) operators which map the current density induced on Γ to the scattered field outside the object, and to the induced current on the scatterer boundary, respectively. As well-known, the radiation operator in (5) is compact and the problem turns to be ill-posed [18], so that regularization strategies are needed to recover a stable and reliable solution [25].

The problem to solve consists in recovering the contour Γ of unknown targets starting from the knowledge of the scattered electric field in a set of measurement points $\boldsymbol{R}_m \in \Sigma$ outside the investigation domain Ω (see Fig. 1). The solution of (5)-(6) requires to face a non-linear problem, since the problem unknown (i.e., the induced current on the scatterers) depends on itself by the MFIE provided in (6). To cope with a simpler task, in literature some simplified approaches have been proposed, considering linearized models of the scattering. The main approximation of the scattering model in case of metallic object is the PO (or *Kirchhoff*). This latter is valid only under some basic assumptions, i.e., *i*) the dimension of the scattering system is large as compared to the operating wavelength in the background medium, *ii*) no mutual scattering occurs between different parts of the scattering system, *iii*) objects should be non convex. The above assumptions lead to assume for the surface current density the form

$$J_{PO}(\boldsymbol{\rho}) \approx 2\hat{\mathbf{n}} \times \boldsymbol{H}_i(\boldsymbol{\rho}) \cdot \hat{\mathbf{z}}, \tag{7}$$

wherein $\hat{\mathbf{n}}$ is the outwardly-oriented normal unit vector to the boundary Γ, and $\boldsymbol{H}_i$ is the in-plane vector magnetic field impinging on scatterer boundaries. This simplification of the scattering model allows resorting to a linear problem solution that can be afforded by means of two approaches we are going to describe in the next paragraphs.

A. BACK-PROPAGATION INVERSION SCHEME

The back-propagation (BCKP) algorithm [18] assumes that the induced current is proportional to the back-propagated field. It aims at finding a minimum least-square pseudo-inverse solution to data equation (5), expressed in a discretized matrix-vector form, i.e.,

$$\underset{\mathbf{J}}{\operatorname{argmin}} \|\mathbf{E}_s - \mathbf{A}_\Sigma \mathbf{J}\|^2. \tag{8}$$

It can be shown that the direct solution of (8) is provided by [18]

$$\tilde{\mathbf{J}}_{BP} = \frac{\left\|\mathbf{A}_\Sigma^+ \mathbf{E}_s\right\|^2_{L^2(\Omega)}}{\left\|\mathbf{A}_\Sigma \mathbf{A}_\Sigma^+ \mathbf{E}_s\right\|^2_{L^2(\Sigma)}} \mathbf{A}_\Sigma^+ \mathbf{E}_s, \tag{9}$$

$\mathbf{A}_\Sigma^+$ being the adjoint of the radiation operator $\mathbf{A}_\Sigma$, whereas Ω and Σ denote investigation and measurement domains on which $L^2(\cdot)$ norm is applied, respectively. Finally, by combining all incident views N_v, the support of induced current is visualised by plotting the square norm of $\tilde{\mathbf{J}}_{BP}$.

B. PHYSICAL OPTICS TRUNCATED SINGULAR VALUE DECOMPOSITION INVERSION SCHEME

A possibility to exploit PO approximation aims at finding the support of the induced current by solving the data equation (5) in a distributional sense through the singular value decomposition of the relevant integral operator mapping data-to-unknown relationship. By introducing the PO approximation (7) and the single layer distribution function with density J, denoted by $J\delta_\Gamma$ [25], the scattered electric field can be rewritten as

$$E_s(\boldsymbol{R}_m) \simeq \int_\Omega G(\boldsymbol{R}_m, \boldsymbol{\rho}'') J_{PO}(\boldsymbol{\rho}'') \delta_\Gamma(\boldsymbol{\rho}'') d\boldsymbol{\rho}'' \tag{10}$$

so that by introducing

$$\gamma(\boldsymbol{\rho}) = -\left[\hat{\mathbf{n}}(\boldsymbol{\rho}) \cdot \hat{\mathbf{k}}_{inc}(\boldsymbol{\rho})\right] U\left[-\hat{\mathbf{n}}(\boldsymbol{\rho}) \cdot \hat{\mathbf{k}}_{inc}(\boldsymbol{\rho})\right] \delta_\Gamma(\boldsymbol{\rho}), \tag{11}$$

eq. (10) can be further expressed as

$$E_s(\boldsymbol{R}_m) \simeq \frac{2}{\zeta_0} \int_\Omega G(\boldsymbol{R}_m, \boldsymbol{\rho}'') \gamma(\boldsymbol{\rho}'') E_{inc}(\boldsymbol{\rho}'') d\boldsymbol{\rho}'', \tag{12}$$

wherein the unknown function $\gamma(\boldsymbol{\rho})$ has compact support included within the scatterer's illuminated side [26], $\hat{\mathbf{k}}_{inc}$ being the local unit vector associated to the incident field and $U(\cdot)$ denoting the Heaviside function, which accounts for the shadowed side of the scatterer. Accordingly, the solution of (12) is given by associating the induced current support to points where the retrieved unknown assumes its largest values in the investigation domain.

The solution of (12) can be conveniently sought by means of a truncated singular value decomposition (TSVD) of the scattering operator. Indeed, a solution of the vector-matrix equation

$$\mathbf{S}\boldsymbol{\gamma} = \mathbf{E}_s, \tag{13}$$

is given by

$$\boldsymbol{\gamma} = \sum_{n=0}^{N_T} \frac{1}{\sigma_n} \langle \mathbf{E}_s, \mathbf{u}_n \rangle_{L^2(\Sigma)} \mathbf{v}_n \tag{14}$$

wherein $\{\mathbf{u}_n, \sigma_n, \mathbf{v}_n\}$ denote the singular system of the compact operator $\mathbf{S}$ [18], and N_T is the cutoff value introduced to find a regularized solution to the ill-posed inverse scattering problem. In the following numerical section we will give addition details about the choice of N_T and the proper visualization of the unknown $\boldsymbol{\gamma}$. In the following we refer to such an inversion approach as PO-TSVD solution.

IV. NUMERICAL RESULTS

Three test cases have been considered to give a proof-of-concept of the advantages of using Bessel-shaped focused beam in imaging the support of metallic targets via linearized inversion. The scattered field data have been generated by the 2D module of COMSOL Multiphysics, considering both single-view and multi-view illumination, while the scattered field data are collected in multi-static configuration by considering $N_m = 72$ equally spaced measurements on a

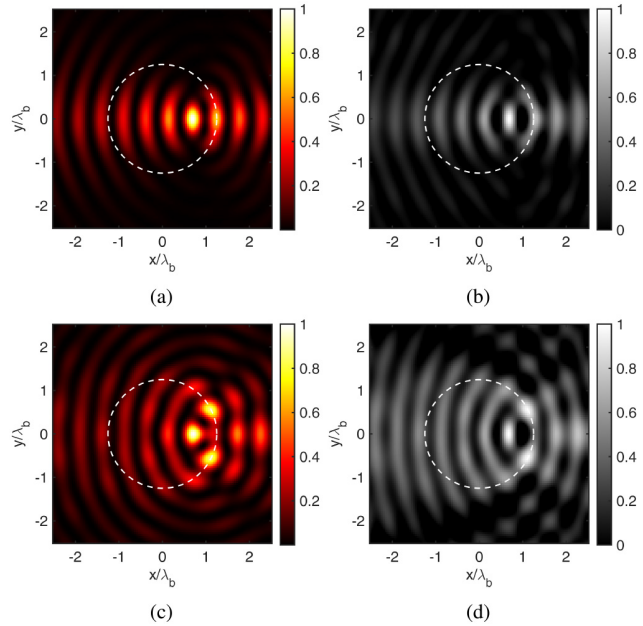

FIGURE 4. Reconstruction of a small PEC cylinder: (a) BCKP and (b) PO-TSVD by means of Bessel-shaped Field illumination, (c) BCKP and (d) PO-TSVD by means of plane-wave illumination.

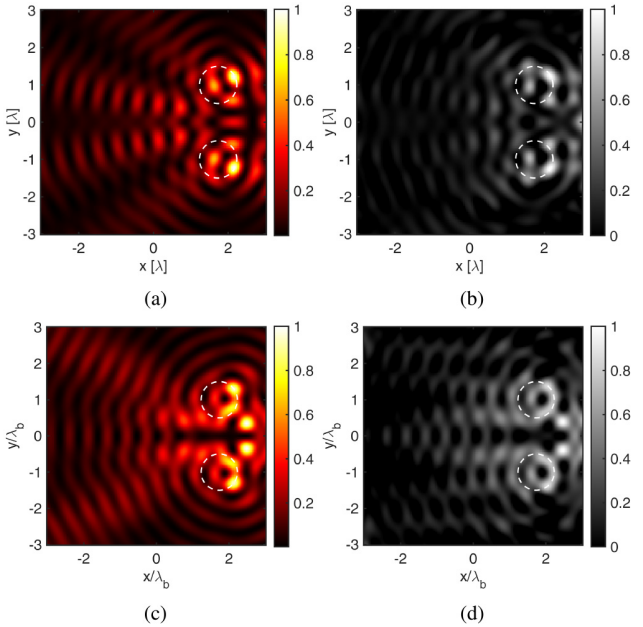

FIGURE 5. Reconstruction of a two small PEC cylinders: (a) BCKP and (b) PO-TSVD by means of Bessel-shaped Field illumination, (c) BCKP and (d) PO-TSVD by means of plane-wave illumination.

circumference of radius 6λ and corrupted by additive white gaussian noise (AWGN) with SNR = 30dB. The incident BF features have been set according to Section II-A. The reconstructions have been performed through the BCKP and PO-TSVD techniques, in the latter case the truncation index N_T has been chosen by finding the index of the first singular value lower than 20dB of the largest one. Finally, according to [25], the support of the induced current can be appraised by plotting only the negative values of the real part of the regularized solution $\boldsymbol{\gamma}$ over the investigation domain Ω.

A. SMALL CIRCULAR CYLINDER

A cylinder of radius 1.25λ is placed at the center of the investigation domain. The BF incident field is that shown in Fig. 2. In Fig. 4(a)-(b) are reported the BCKP and PO-TSVD reconstructions. As it can bee seen, both the approaches are able to retrieve the side of the illuminated target although many artifacts are present in the investigation domain, due to resolution limits associated to the reconstruction of a δ-pulse along the field incident direction, that results in a ghost patches not corresponding to the actual boundaries of the targets. On the other hand, if the reconstruction is compared with that obtained through single-view plane-wave propagating towards $-\hat{x}$ (0° degrees), see Fig. 4(c)-(d), better result achieved by BF illumination can be highlighted, since the PW reconstruction clearly shows some artifacts resembling two different small scatterers, and does not reveal the continuous cylinder's boundary. This is related to the bad approximation given by physical optics in presence of a small cylinder [18]. Conversely, BF illumination provides a better approximation in terms of PO, as shown in [19], and this explains why the associated reconstruction provides better results than standard PW illumination. Last but not least, the reconstruction related to PW shows much more relevant blurring effects than those achieved through BF in the whole investigation domain.

B. TWO SMALL CIRCULAR CYLINDER

In this example, two circular cylinders of radius 0.5λ are spaced one wavelength and illuminated by two BFs impinging with beam axis directed along $\phi = \pm 30°$ (see Fig. 1). The reconstructions are reported in Fig. 5. Also in this case BF illuminations provide better results, especially with PO-TSVD inversion, since the BF allows imaging the illuminated boundaries of the cylinders without relevant blurring effects in the imaging domain. On the other hand, PW reconstruction clearly shows two ghost artifacts between the cylinders, due to multiple scattering effects arising from closely-spaced targets.

C. "C-SHAPED" CYLINDER

The last example is concerned with a C-shaped metallic target with a leading dimension of 4λ. In this case, the incident field (BF and PW) impinges toward the investigation domain with an angle of $\phi = -45°$. As expected, the BCKP solution is completely unreliable as it can be inferred from Figs. 6(a) and 6(c), since the large extent of the target prevents to profitably use this kind of inversion technique. On the other hand, the PO-TSVD allows appraising the illuminated side (lower part) of the target while keeping low the blurring effects in the whole region of interest (Fig. 6(b)). Interestingly, if we consider reconstructions obtained with PW illumination, it is almost impossible to detect any feature of the scatterer, resulting in a completely blurred image, see Fig. 6(d).

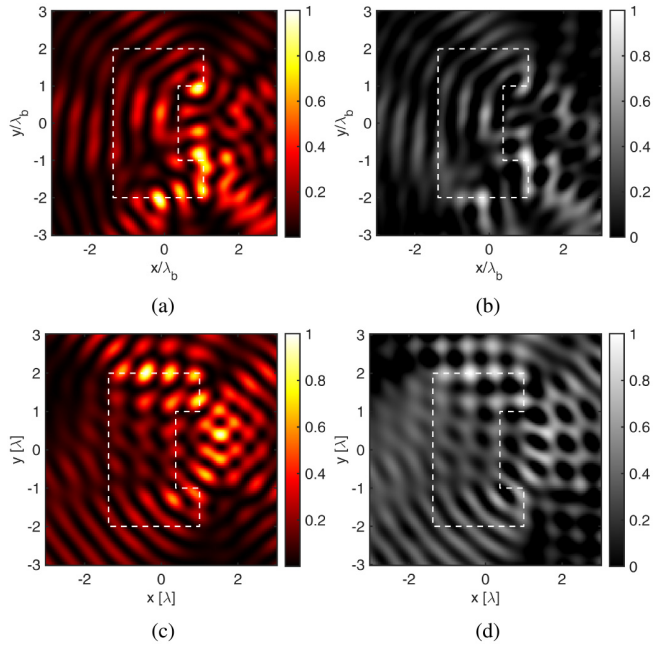

FIGURE 6. Reconstruction of a C-shaped PEC cylinder: (a) BCKP and (b) PO-TSVD by means of Bessel-shaped Field illumination, (c) BCKP and (d) PO-TSVD by means of plane-wave illumination.

V. CONCLUSION

In this work, we dealt with forward and inverse scattering of metallic objects by focused Bessel-shaped incident field. The focusing capabilities of such an incident field were investigated to understand whether this kind of fields can improve shape reconstruction of metallic targets not so far extended with respect to probing wavelength, thus not satisfying the requirements underlying physical optics approximation. Numerical full-wave examples and linear inversion algorithms based on back-propagation and physical optics revealed better focused reconstructions when Bessel-shaped fields are used as incident field, especially when compared to standard incident plane wave. Further investigations will be addressed to exploit these kinds of focused fields in realistic measurement configurations comprising subsurface GPR and millimeter wave, radar imaging exploiting multifrequency data, as well as full-aspect data surveys concerned with non standard circular or spherical array configurations. Possible extensions to vector and 3D electromagnetic scattering will be also considered.

ACKNOWLEDGMENT

Santi C. Pavone would like to acknowledge the Project PON-AIM "Attraction and International Mobility" by the Italian Ministry of University and Research (MUR) and PIACERI starting grant (quota 2D) from the University of Catania. G. Sorbello and L. Di Donato would like to acknowledge PIACERI project "Voltmeter" funded by University of Catania.

REFERENCES

[1] J. Lu and J. F. Greenleaf, "Ultrasonic nondiffracting transducer for medical imaging," *IEEE Trans. Ultrason., Ferroelect., Freq. Control*, vol. 37, no. 5, pp. 438–447, Sep. 1990.

[2] K.-S. Lee and J. P. Rolland, "Bessel beam spectral-domain high-resolution optical coherence tomography with micro-optic axicon providing extended focusing range," *Opt. Lett.*, vol. 33, no. 15, pp. 1696–1698, 2008.

[3] T. A. Planchon *et al.*, "Rapid three-dimensional isotropic imaging of living cells using Bessel beam plane illumination," *Nat. meth.*, vol. 8, no. 5, pp. 417–423, 2011.

[4] A. F. Valle and J. D. Seelig, "Two-photon Bessel beam tomography for fast volume imaging," *Opt. Exp.*, vol. 27, no. 9, pp. 12147–12162, 2019.

[5] C. Liu *et al.*, "High-speed, multi-modal, label-free imaging of pathological slices with a Bessel beam," *Biomed. Opt. Exp.*, vol. 11, no. 5, pp. 2694–2704, 2020.

[6] D. Mugnai and P. Spalla, "Electromagnetic propagation of Bessel-like localized waves in the presence of absorbing media," *Opt. Commun.*, vol. 282, no. 24, pp. 4668–4671, 2009.

[7] A. Mazzinghi *et al.*, "Large depth of field pseudo-Bessel beam generation with a RLSA antenna," *IEEE Trans. Antennas Propag.*, vol. 62, no. 8, pp. 3911–3919, Aug. 2014.

[8] M. Ettorre, S. C. Pavone, M. Casaletti, M. Albani, A. Mazzinghi, and A. Freni, "Near-field focusing by non-diffracting Bessel beams," in *Aperture Antennas for Millimeter and Sub-Millimeter Wave Applications*. Heidelberg, Germany: Springer, 2018, pp. 243–288.

[9] S. Chen *et al.*, "Demonstration of 20-Gbit/s high-speed bessel beam encoding/decoding link with adaptive turbulence compensation," *Opt. Lett.*, vol. 41, no. 20, pp. 4680–4683, 2016.

[10] J. Arlt, V. Garcés-Chávez, W. Sibbett, and K. Dholakia, "Optical micromanipulation using a Bessel light beam," *Opt. Commun.*, vol. 197, nos. 4–6, pp. 239–245, 2001.

[11] D. McGloin and K. Dholakia, "Bessel beams: Diffraction in a new light," *Contemp. Phys.*, vol. 46, no. 1, pp. 15–28, 2005.

[12] H. E. Hernández-Figueroa, M. Zamboni-Rached, and E. Recami, *Localized Waves*, vol. 194. Hoboken, NJ, USA: Wiley, 2008.

[13] H. E. Hernández-Figueroa, M. Zamboni-Rached, and E. Recami, *Non-Diffracting Waves*. Hoboken, NJ, USA: Wiley, 2013.

[14] W. Fuscaldo and S. C. Pavone, "Metrics for localized beams and pulses," *IEEE Trans. Antennas Propag.*, vol. 68, no. 2, pp. 1176–1180, Feb. 2020.

[15] J. Durnin, "Exact solutions for nondiffracting beams. I. The scalar theory," *JOSA A*, vol. 4, no. 4, pp. 651–654, 1987.

[16] J. Durnin, J. Miceli, Jr., and J. Eberly, "Diffraction-free beams," *Phys. Rev. Lett.*, vol. 58, no. 15, p. 1499, 1987.

[17] M. Bertero and P. Boccacci, *Introduction to Inverse Problems in Imaging*. Bristol, U.K.: Inst. Phys., 1998.

[18] A. J. Devaney, *Mathematical Foundations of Imaging, Tomography and Wavefield Inversion*. Cambridge, U.K.: Cambridge Univ. Press, 2012.

[19] S. C. Pavone, G. Sorbello, and L. Di Donato, "Improving physical optics approximation through Bessel beam scattering," *IEEE Antennas Wireless Propag. Lett.*, vol. 20, no. 6, pp. 993–997, Jun. 2021.

[20] C. A. Balanis, *Advanced Engineering Electromagnetics*. Hoboken, NJ, USA: Wiley, 2012.

[21] S. C. Pavone, M. Ettorre, M. Casaletti, and M. Albani, "Analysis and design of Bessel beam launchers: Transverse polarization," *IEEE Trans. Antennas Propag.*, vol. 69, no. 8, pp. 5175–5180, Aug. 2021.

[22] O. Brzobohatỳ, T. Čižmár, and P. Zemánek, "High quality quasi-Bessel beam generated by round-tip axicon," *Opt. Exp.*, vol. 16, no. 17, pp. 12688–12700, 2008.

[23] S. Monk, J. Arlt, D. Robertson, J. Courtial, and M. Padgett, "The generation of bessel beams at millimetre-wave frequencies by use of an axicon," *Opt. Commun.*, vol. 170, nos. 4–6, pp. 213–215, 1999.

[24] S. C. Pavone, A. Mazzinghi, A. Freni, and M. Albani, "Comparison between broadband bessel beam launchers based on either Bessel or Hankel aperture distribution for millimeter wave short pulse generation," *Opt. Exp.*, vol. 25, no. 16, pp. 19548–19560, 2017.

[25] R. Pierri, A. Liseno, and F. Soldovieri, "Shape reconstruction from PO multifrequency scattered fields via the singular value decomposition approach," *IEEE Trans. Antennas Propag.*, vol. 49, no. 9, pp. 1333–1343, Sep. 2001.

[26] R. Pierri, A. Liseno, R. Solimene, and F. Soldovieri, "Beyond physical optics SVD shape reconstruction of metallic cylinders," *IEEE Trans. Antennas Propag.*, vol. 54, no. 2, pp. 655–665, Feb. 2006.